Creation of multiple nanodots by single ions

ENDER AKCÖLTEKIN[1], THORSTEN PETERS[1], RALF MEYER[1], ANDREAS DUVENBECK[1], MIRIAM KLUSMANN[1], ISABELLE MONNET[2], HENNING LEBIUS[2] AND MARIKA SCHLEBERGER[1]*

[1]Universität Duisburg-Essen, FB Physik, 47048 Duisburg, Germany
[2]CIRIL (CEA, CNRS, ENSICAEN), 14070 Caen Cedex 5, France
*e-mail: marika.schleberger@uni-due.de

Published online: 29 April 2007; doi:10.1038/nnano.2007.109

In the search to develop tools that are able to modify surfaces on the nanometre scale, the use of heavy ions with energies of several tens of MeV is becoming more attractive. Low-energy ions are mostly stopped by nuclei, which causes the energy to be dissipated over a large volume. In the high-energy regime, however, the ions are stopped by electronic excitations[1–3], and the extremely local ($\sim$10 nm^3) nature of the energy deposition leads to the creation of nanosized 'hillocks' or nanodots under normal incidence[4–6]. Usually, each nanodot results from the impact of a single ion, and the dots are randomly distributed. Here we demonstrate that multiple, equally spaced dots, each separated by a few tens of nanometres, can be created if a single high-energy xenon ion strikes the surface at a grazing angle. By varying this angle, the number of dots, as well as their spacing, can be controlled.

We studied this process in single crystals of strontium titanate ($SrTiO_3$). This ferroelectric oxide has a perovskite (ABO_3) structure and is widely used as a catalyst[7] and as a substrate material for GaAs solar cells. It is also being discussed as a possible material for nuclear waste management[8], and as a possible insulator of choice in future microelectronic devices because its high dielectric constant leads to very low tunnelling currents compared with SiO_2 (refs 9, 10). $SrTiO_3$ is also used as a substrate for the deposition of high-temperature superconductors. It is possible to increase the critical current densities of these materials by patterning the substrate[11], so the ability to create regular nanosized structures in $SrTiO_3$ could lead to improved performances for superconducting films.

After irradiation under grazing angles of a few degrees with respect to the surface plane, the samples were imaged by atomic force microscopy (AFM) *in situ*, under ultrahigh vacuum conditions. In Fig. 1 we show AFM images of samples, each irradiated under two different incidence angles, resulting in different types of defects. If irradiated at $\Theta = 6^\circ$, slightly elongated hillocks occur (Fig. 1a). If the angle is changed to $\Theta = 3^\circ$, round, almost evenly spaced, hillocks appear, which are still overlapping (Fig. 1a). At angles smaller than $\Theta = 3^\circ$, the dots are clearly separated and the tracks look like pearls on a chain, as can be seen in Fig. 1b (this sample was irradiated at $\Theta = 1^\circ$ and at $\Theta = 2^\circ$). The number of chains corresponds to the number of ions. This means that each chain containing dozens of nanodots is created by a single ion travelling through the solid. From analysing more than 600 individual chains irradiated under different angles Θ, we found that the length l of the chains can be controlled by varying the angle of incidence, as can be seen in Fig. 2. At $\Theta = 1^\circ$, most of the chains are already about half a micrometre in length. The average height we find for all chains stemming from irradiations at incidence angles of less than 3° is 2.5 ± 1.0 nm. They are of circular shape with a diameter (full-width-at-half-maximum, FWHM) of 25 ± 5 nm. The distance between individual hillocks depends on the angle of incidence; for example, for the marked chain in Fig. 1b it is 35 ± 3 nm. Similar measurements (not shown here) on irradiated TiO_2 and Al_2O_3 show the same chains of dots as on $SrTiO_3$. We take this as an indication that the phenomenon may be typical not only for perovskites but also of other oxidic materials.

To date, the patterning of ferroelectric oxides has been achieved by self-organizing 'bottom-up' approaches[12,13] as well as by top-down methods such as lithography using low-energy ions[14], evaporation through a shadow mask[15] or a combination of both[16]. With these techniques the created structures are either randomly distributed or shaped, or the periodicity is limited to 100 nm at best. To our knowledge, no other technique that is able to create regular-shaped nanodots on a perovskite surface with a spacing of 35 nm has so far been established.

In order to describe the ion–solid interaction the so-called thermal spike (TS)-model has been developed[17]. It has been applied to the special case of swift heavy ions, where electronic stopping dominates over nuclear stopping by several orders of magnitude[18]. It describes the formation of cylindrical tracks of amorphous or recrystallized material inside the solid. It does not explain the formation mechanism of hillocks on the surface, nor the formation of hillock chains. The starting point to gain an understanding of the formation of nanodot chains on $SrTiO_3$ may be found in early experiments with van der Waals materials such as MoS_2 or WSe_2. In these materials, intermittent fission tracks have been observed by transmission electron microscopy[19]. These discontinuous tracks were explained by the strong spatial anisotropy of a van der Waals crystal lattice. The π-electrons are fully contained within the crystal planes and there is only a weak hydrogen bond between the planes. Each time the projectile hits a lattice plane with a high density of electrons, enhanced electronic stopping occurs. This significant anisotropy leads to periodic spikes of radiation damage in this type of material. Such a triggered loss process could also explain the distinct features we observe.

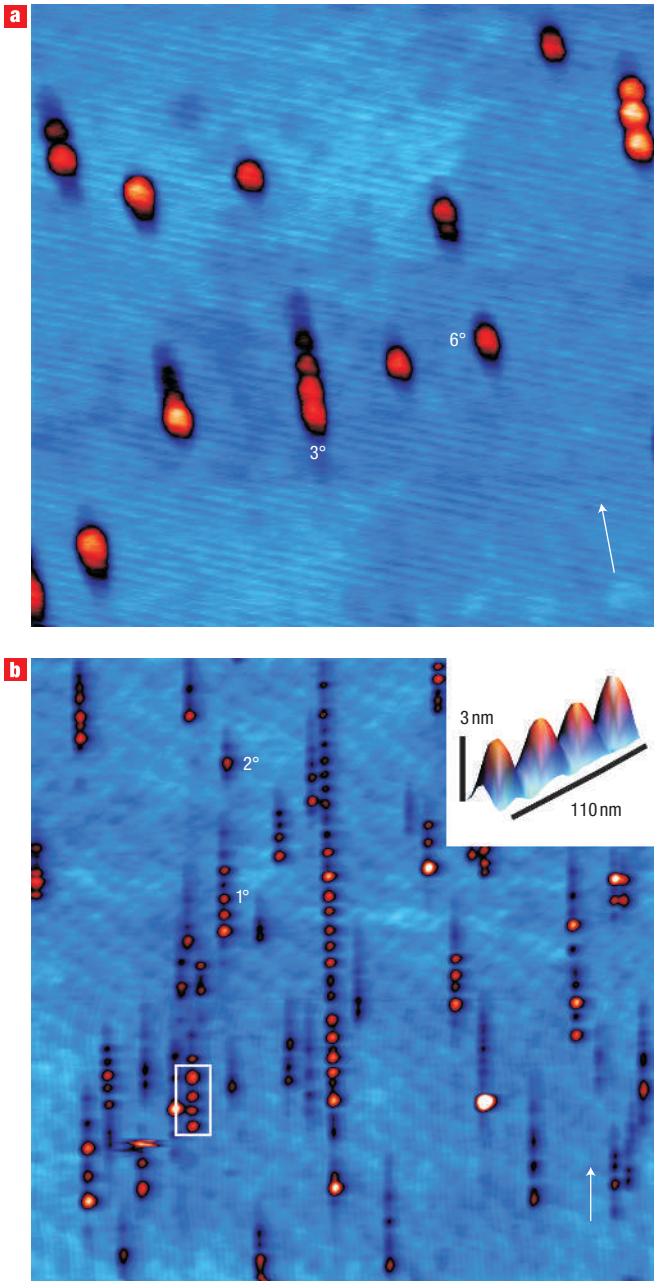

Figure 1 AFM images of nanodots and chains on $SrTiO_3$ created by irradiation. Both samples were irradiated twice with 92 MeV Xe ions. **a**, Image for angles of incidence of $\Theta = 3°$ and $\Theta = 6°$. Each dot or chain corresponds to a single ion hit. **b**, The longer chains stem from irradiation at $\Theta = 1°$ and the shorter chains from irradiation at $\Theta = 2°$. The inset shows the size and shape of the individual dots within a chain. Frame size is 500×500 nm^2 in **a** and $1{,}300 \times 1{,}300$ nm^2 in **b**. To enhance the contrast, false colouring was used. Colour changing from blue to red to white corresponds to the height, varying from 0 to 4.4 nm (**a**) and from 0 to 3.7 nm (**b**), respectively. The arrows indicate the direction of the incoming ions.

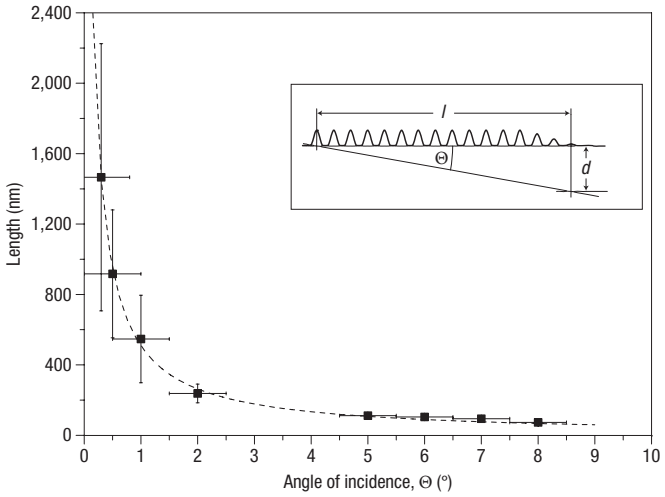

Figure 2 Measured length *l* of chains as a function of angle of incidence. The dashed line is a fit, according to our model, with depth $d = 9.8$ nm. Error bars denote the reproduceability (angle) as well as the measured distribution width (length).

If the ion travels through $SrTiO_3$ it will continuously interact with the electrons in the material, but energy loss is more probable where the electron density is high. In this case, the sudden interaction of the projectile with the electrons gives rise to a sharply peaked energy distribution. How this electronic excitation finally leads to the modification of the material (craters, hillocks, tracks and so on) is still not exactly known. The TS-model describes the energy transport out of the electronically heated region, whereas the Coulomb explosion model[20] couples the electron excitation to atomic motion caused by the repulsive forces acting in the transiently ionized region. Both models cover important aspects of the creation processes for material modifications[21]. In our experiment the strong ionization rate of the swift heavy ion leads to a significant charge imbalance. From an empirical formula[22] and extrapolation of experimental data[23], we find that Xe ions moving through $SrTiO_3$ with 92 MeV have an effective equilibrium charge close to the original charge state of 23. However, our data do not allow us to make a clear correlation with either of the two scenarios. For both models to be predictive, the initial conditions need to be known. A strong anisotropy of the electronic structure as, for example, in a van der Waals material, will influence the loss process significantly, whether it is connected to either a Coulomb explosion or to a thermal spike.

Note, however, that $SrTiO_3$ is not a van der Waals material and the observed features cannot be simply attributed to the ion crossing crystal layers of a homogeneous electron density. If the anisotropy was exclusively parallel to the surface (as is the case with MoS_2), we would observe that the number of nanodots was constant and the distance between dots would vary as a function of the angle of incidence. If the anisotropy was exclusively normal to the surface, we would observe a varying number of dots, but the distance between them would be constant. In our case the anisotropy is given parallel as well as normal to the surface. Therefore, the observed distance between dots and the number of the dots as a result of a triggered loss process needs to be discussed taking the full three-dimensional electronic structure into account. To this end, we performed *ab initio* density functional theory (DFT, see Theory section, Methods) calculations to determine the electronic density of $SrTiO_3$ and derived the density along the path of the travelling ion.

Most of the electrons are located around the oxygen atoms and the density is higher in the TiO_2 planes than in the SrO planes (Fig. 3). Simple geometrical considerations taking the electron

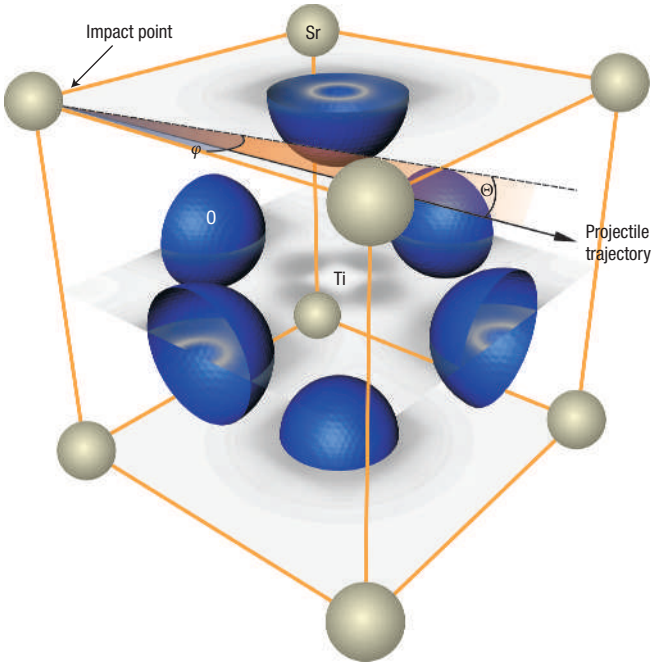

Figure 3 DFT calculation of the electron density of $SrTiO_3$. The grey shading represents electron density. Atom positions (apart from the central titanium atom) are also visualized. The arrow indicates a possible projectile trajectory defined by the azimuthal angle φ as well as the incidence angle Θ.

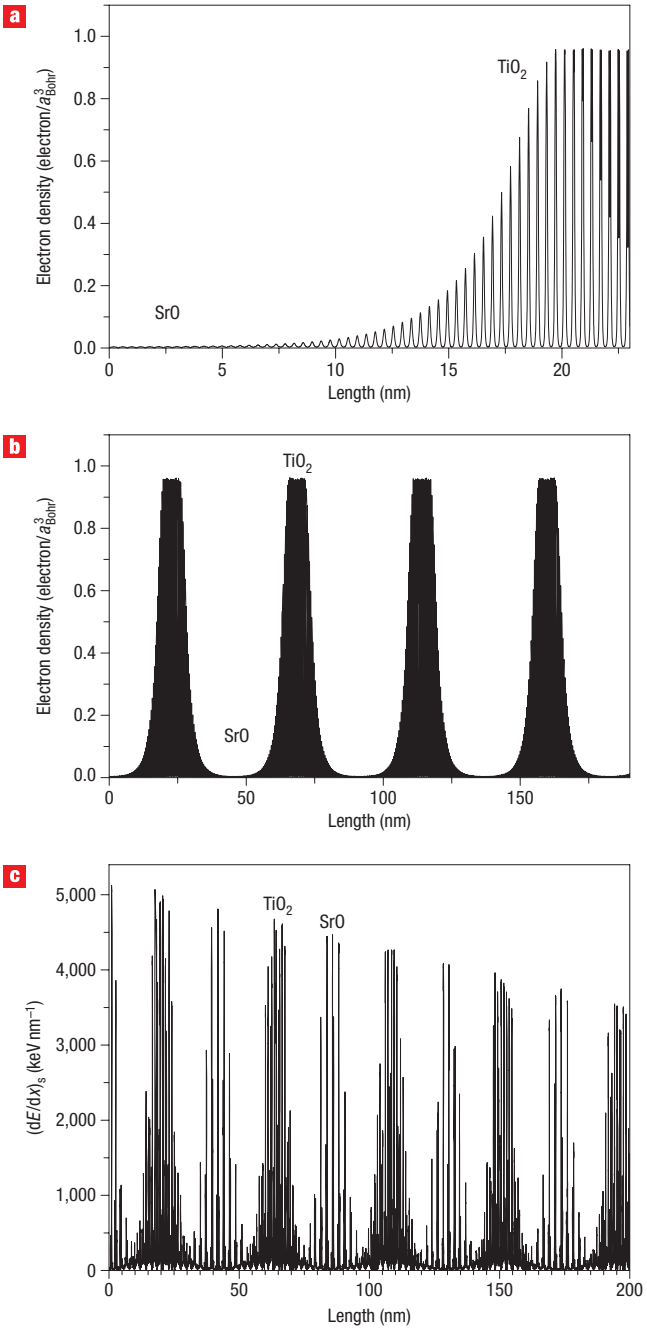

Figure 4 Electron density and electronic stopping. a,**b**, Simulation of the electron density that the ion encounters when travelling through the crystal lattice at a grazing angle of $\Theta = 0.5°$ with respect to the (100) surface plane of a $SrTiO_3$ single crystal (Fig. 3). Panel **a** shows the leftmost part of **b** in more detail. The peaks in **a** stem from a crystal unit cell; the peaks in **b** stem from a crystal layer. **c**, Electronic stopping $(dE/dx)_s$ along the track of a Xe projectile hitting a $SrTiO_3$ single crystal with $\Theta = 0.5°$ and $\varphi = 10°$.

density into account yield a very good qualitative agreement with the periodic defects occuring in $SrTiO_3$, as can be seen from Fig. 4a, b. We used the DFT data to calculate the electron density encountered by an ion following a typical trajectory through a perfect $SrTiO_3(100)$ crystal under a grazing angle of $\Theta = 0.5^\circ$ and an azimuthal angle of $\varphi = 0^\circ$ (Fig. 3). On its way through a single lattice plane, the ion interacts with the electrons of several dozens of oxygen atoms. Each peak in the fine structure (Fig. 4a) is due to the interaction of the ion with the electrons surrounding one oxygen atom. The sum of these interactions within one crystal plane (Fig. 4b) creates a strong local excitation, leading finally to a nanodot on the surface. The ion then typically travels several hundred Ångström through the crystal without energy loss before it again encounters an area with a high enough electron density.

Even though the exact mechanisms of the observed dot formation are not known, we may assume the space- and time-dependent generation of excitation energy $E_s(\mathbf{r}, t)$ along the trajectory of the projectile $\mathbf{r}_p(t)$ as well as the transport of excitation energy to play a key role in that process. It should be emphasized here that reduction of the problem to radial symmetry with respect to the swift heavy-ion track, as is usual in TS-model calculations[24], is not allowed in our case owing to (1) the consideration of the local electron density on a sub-Ångström length scale and (2) the necessity for the correct incorporation of the surface plane into the excitation energy transport process. In contrast to the TS-model calculations, we propose to perform a nested two-step calculation approach (see Theory section, Methods).

In the present study we focus our interest on the striking periodicity of the nanodots, which should already be present in the space dependence of the electronic stopping (ES) along the trajectory $(dE/dx)_s$ derived from $(dE_s/dt)(\mathbf{r}_p(t))$, (see Theory section, Methods). Figure 4c shows the result of an exemplary calculation of this ES for a 0.71 MeV u^{-1} Xe projectile hitting a perfect $SrTiO_3$ crystal under $\Theta = 0.5^\circ$ and $\varphi = 10^\circ$. Two kinds of peaks can be seen, one originating from the TiO_2 planes, the second one from the SrO planes. The average ES in the TiO_2 planes is higher by a factor of 2 (integrating over the peak area).

Thus, for this particular choice of impact parameters, the periodicity of the dot formation may be governed by the contribution of the TiO_2 planes. The decrease of the maximum peak heights with increasing track length L due to electronic friction will be one factor limiting the total chain length l. A more quantitative discussion of features such as, for example, chain length, track radius and temporal dynamics, goes beyond the scope of this paper, because it would require a detailed analysis of the full four-dimensional excitation energy profile $E(\mathbf{r}, t)$ (see equation (1) in the Theory section, Methods), using the ES discussed above.

Our model is further corroborated by plotting the measured length of the chains as a function of the angle of incidence as shown in Fig. 2. The data can be fitted nicely by using $l(\Theta) = d/\tan\Theta$. Here, l is the length of the chain and d is the maximum depth from where the excitation starts (see inset in Fig. 2). In addition, we frequently observe that at the very end of a chain the height of the dots decreases monotonically. These findings could be explained if we assume that the ion is already travelling too deep below the surface and the material modifications no longer reach the surface. In this way, we can determine the radius of the modified volume from our data. Our value of $\sim$10 nm is larger by a factor of 2 than the effective latent track radii derived from irradiation experiments on different insulators under 90° (refs 25, 26). Repeating our experiment with an amorphous layer of SiO_2, we also find periodic dots[27]. It is not clear, yet, what the origin of this periodicity is, but it could be the electron density, maybe even of the underlying crystalline Si substrate.

In conclusion, we have demonstrated how to produce periodic nanodots on oxidic surfaces by a single ion hit. We propose that the anisotropic electron density of the material gives rise to a triggered energy loss process. The resulting nanodots imaged by AFM thus represent a direct view of the projection of the three-dimensional electronic density onto the surface.

METHODS

EXPERIMENT

The experiments were performed at the beamline IRRSUD of the Grand Accelerateur National d'Ions Lourds (GANIL) in Caen, France. An UHV-AFM/STM (Omicron) was mounted to the chamber where the irradiation took place. The base pressure was 1×10^{-10} mbar in the AFM. As samples we used $SrTiO_3$(100), TiO_2(100) and Al_2O_3(1102) crystals (CrysTec). The samples were cleaned with acetone. We used no etching to remove excess SrO terminations, as this would not play a role in hillock formation. AFM images taken before irradiation to check the cleanliness of the samples often showed atomically flat terraces separated by atomic steps.

The samples were irradiated with a beam of Xe^{23+} ions at 0.71 MeV u^{-1} scanned over the whole surface area of the target. Typically, a fluence of 1×10^9 ions cm^{-2} was chosen, resulting in 10 impacts per μm^2 on average. At this fluence, enough events are produced to obtain good statistics, but the probability that two ions hit the same spot, resulting in nonlinear phenomena, is still sufficiently low. For $SrTiO_3$, the chosen projectile/energy combination results in an energy loss of 19.1 keV nm^{-1} (SRIM; ref. 28). The angle of incidence with respect to the surface was varied between $\Theta = 1°$ and $\Theta = 6°$. The uncertainty of the absolute angle is $\pm1°$. The azimuthal angle φ was not controlled. Immediately after irradiation all samples were measured with the AFM using the contact mode ($F = 0.2$ nN) as well as the dynamic mode ($df = -10$ Hz) *in situ*. Additional data from *ex situ* measurements were used for Fig. 2. No postirradiation treatment was applied. Thus, all observed topographical features can be attributed unambiguously to the irradiation.

All AFM images were recorded with the Omicron SCALA PRO software, version 4.1 and processed with the Nanotec Electronica SL WSxM software, version 4.0, Develop 8.32 (ref. 29). From the raw data (400×400 data points), only a plane was subtracted. The colour code was changed using the palette *flow.lut*. No change of contrast (1) or brightness (0) was used.

THEORY

The DFT calculations were performed using the ABINIT package[30] together with pseudopotentials generated by the fhi98pp code[31] to determine the distribution of the electrons in $SrTiO_3$. For the exchange-correlation energy, the Perdew–Burke–Ernzerhof generalized-gradient approximation functional[32] was used. In a first step, the equilibrium lattice constant of the investigated system was obtained. The result is $7.53a_{\mathrm{Bohr}}$ for $SrTiO_3$. Subsequently the electron density at the equilibrium lattice constant was derived. A common kinetic-energy cutoff energy of 96 Hartree for the expansion of the wavefunctions and a 8×8×8 k-point mesh were used in all calculations.

In the energy regime considered here, the generation of excitation energy can be approximately treated within the frame of the Lindhard model[33] of electronic stopping. Using that framework, the excitation energy $dE_s(\mathbf{r}_p(t))$ that is transferred from the kinetic energy of the projectile into the electronic system within the time interval dt is proportional to the momentary kinetic energy of the projectile and to the local electron density $n_{el}(\mathbf{r}_p(t))$ provided by the *ab initio* DFT calculations as explained above. We assume the time evolution of the four-dimensional profile $E(\mathbf{r}, t)$ of excitation energy within the solid to be described by the diffusion equation

$$\frac{\partial E}{\partial t}(\mathbf{r},t) - D\nabla^2 E(\mathbf{r},t) = \frac{dE_s}{dt}(\mathbf{r}_p(t), E_{kin}(\mathbf{r}_p(t)), n_{el}(\mathbf{r}_p(t))) \qquad (1)$$

where D denotes the diffusion coefficient. The projectile trajectory $\mathbf{r}_p(t)$ entering equation (1) is obtained by numerically integrating the Newtonian equations of motion, including an effective friction term originating from the Lindhard treatment.

A straight forward numerical treatment of equation (1) is hampered by the complexity of the problem. On the one hand, the lateral dimensions of the observed nanodots are of the order of several tens of nanometres; on the other hand, the electron density within one unit cell varies on the sub-Ångström length scale. Therefore, a nested two-step calculation approach was used. In the first step, we take advantage of the straightness of the ion track and—for given impact parameters (Θ, φ)—geometrically determine the set of intersection points through the unit cells along the trajectory of the projectile. This procedure is performed for a total trajectory length L that corresponds to a laterally projected range larger than the observed period length of the nanodots. Beginning with the unit cell at the impact point, each traversed cell is discretized into more than 10^5 voxels to match the sub-Ångström resolution of $n_{el}(\mathbf{r}, t)$. A numerical integration of the equations of motion of the projectile using the highly resolved electron density yields the total generated excitation energy $dE_s(\mathbf{r}_p(t))$ as well as the travelling time dt for that cell. Naturally, the kinetic energy of the heavy ion is reduced after traversing one cell owing to electronic stopping.

This reduced energy, as well as the exit point of one cell, are taken as the new initial parameters for the analogous calculation carried out for the subsequent cell. Iteration of this algorithm yields a set of $(dE/dt)_i$, which in the second step of our model, is treated as distinct point sources of excitation energy in a discrete representation of equation (1), with a grid-spacing in units of one elementary cell. Using this coarse discretization, the numerical solution of equation (1) can be obtained using a Green's functions approach for the half-space diffusion problem.

Received 30 January 2007; accepted 26 March 2007; published 29 April 2007.

References

1. Bethe, H. Zur Theorie des Durchgangs schneller Korpuskularstrahlen durch Materie. *Ann. Phys.* **397,** 325–400 (1930).
2. Bloch, F. Zur Bremsung rasch bewegter Teilchen beim Durchgang durch Materie. *Ann. Phys.* **408,** 285–320 (1933).
3. Lindhard, J., Scharff, M. & Schiøtt, H. E. Range concepts and heavy ion ranges (Notes on atomic collisions, II). *Mat. Fys. Medd. Dan. Vid. Selsk.* **33,** 1–42 (1963).
4. Neumann, R. Scanning probe microscopy of ion-irradiated materials. *Nucl. Instrum. Methods B* **151,** 42–55 (1999).
5. Bouffard, S., Cousty, J., Pennec, Y. & Thibaudau, F. STM and AFM observations of latent tracks. *Radiat. Eff. Defects Solids* **126,** 225–228 (1993).
6. Khalfaoui, N., Görlich, M., Müller, C., Schleberger, M. & Lebius, H. Latent tracks in CaF_2 studied with atomic force microscopy in air and in vacuum. *Nucl. Instrum. Methods B* **245,** 246–249 (2006).
7. Li, R., Tang, Q., Yin, S. & Sato, T. Plasma catalysis for CO_2 decomposition by using different dielectric materials. *Fuel Processing Technol.* **87,** 617–622 (2006).
8. Thevuthasan, S., Shutthanandan, V. & Zhang, Y. Applications of high energy ion beam techniques in environmental science: Investigation associated with glass and ceramic waste forms. *J. Electr. Spectr. Rel. Phen.* **150,** 195–207 (2006).
9. Jeon, S., Walker, F. J., Billman, C. A., McKee, R. A. & Hwang, H. Electrical characteristics of epitaxially grown $SrTiO_3$ on silicon for metal–insulator–semiconductor gate dielectric applications. *IEEE Electron. Device Lett.* **24,** 218–220 (2003).

10. Först, C. J., Ashman, C. R., Schwarz, K. & Blöchl, P. E. The interface between silicon and a high-*k* oxide. *Nature* **427,** 53–56 (2004).
11. Brück, S. & Albrecht, J. Experimental evidence of the dominant role of low-angle grain boundaries for the critical current density in epitaxially grown $YBa_2Cu_3O_{7-\delta}$ thin films. *Phys. Rev. B* **71,** 174508 (2005).
12. Zhang, M. *et al*. Patterned nanoclusters in the indium-doped $SrTiO_3$ films. *Appl. Phys. Lett.* **85,** 5899–5901 (2004).
13. Szafraniak, I. *et al*. Ferroelectric epitaxial nanocrystals obtained by a self-patterning method. *Appl. Phys. Lett.* **83,** 2211–2213 (2003).
14. Albrecht, J. *et al*. Surface patterning of $SrTiO_3$ by 30 keV ion irradiation. *Surf. Sci.* **547,** L847–L852 (2003).
15. Shin, H.-J. *et al*. Patterning of ferroelectric nanodot arrays using a silicon nitride shadow mask. *Appl. Phys. Lett.* **87,** 113114 (2005).
16. Ruzmetov, D. *et al*. Epitaxial magnetic perovskite nanostructures. *Adv. Mater.* **17,** 2869–2872 (2005).
17. Seitz, F. & Koehler, J. S. Displacement of atoms during irradiation, in *Solid State Physics: Advances in Research and Applications 2,* (eds Seitz, F. & Turnbull, D.) 305–448 (1956).
18. Toulemonde, M., Dufour, C. & Paumier, E. Transient thermal process after a high-energy heavy-ion irradiation of amorphous metals and semiconductors. *Phys. Rev. B* **46,** 14362–14369 (1992).
19. Morgan, D. V. & Chadderton, L. T. Fission fragment tracks in semiconducting layer structures. *Phil. Mag.* **17,** 1135–1143 (1968).
20. Fleischer, R. L., Price, P. B. & Walker, R. M. Ion explosion spike mechanism for formation of charged-particle tracks in solids. *J. Appl. Phys.* **36,** 3645–3652 (1965).
21. Klaumünzer, S. Ion tracks in quartz and vitreous silica. *Nucl. Instrum. Methods B* **225,** 136–153 (2004).
22. Shima, K., Ishihara, T., Miyoshi, T. & Mikumo, T. Equilibrium charge-state distributions of 35–146-MeV Cu ions behind carbon foils. *Phys. Rev. A* **28,** 2162–2168 (1983).
23. Shima, K., Kuno, N. & Yamanouchi, M. Systematics of equilibrium charge distributions of ions passing through a carbon foil over the ranges $Z = 4–92$ and $E = 0.02–6$ MeV/u. *Phys. Rev. A* **40,** 3557–3570 (1989).
24. Toulemonde, M., Dufour, C. & Paumier, E. The ion–matter interaction with swift heavy ions in the light of inelastic thermal spike model. *Acta Physica Polonica A* **109,** 311–322 (2006).
25. Meftah, A. *et al*. Track formation in SiO_2 quartz and the thermal-spike mechanism. *Phys. Rev. B* **49,** 12457–12463 (1994).
26. Szenes, G. General features of latent track formation in magnetic insulators irradiated with swift heavy ions. *Phys. Rev. B* **51,** 8026–8029 (1995).
27. Carvalho, A. M. J. F. *et al*. Discontinuous ion tracks on silicon oxide on silicon surfaces after grazing-angle heavy ion irradiation. *Appl. Phys. Lett.* **90,** 073116 (2007).
28. Ziegler, J. F. & Biersack, J. P. The stopping and range of ions in matter; http://www.SRIM.org, Version 2003.26.
29. Horcas, I. *et al*. A software for scanning probe microscopy and a tool for nanotechnology. *Rev. Sci. Instr.* **78,** 013705 (2007).
30. The abinit code is a common project of the Université Catholique de Louvain, Corning Incorporated, and other contributors. http://www.abinit.org
31. Fuchs, M. & Scheffler, M. Ab initio pseudopotentials for electronic structure calculations of poly-atomic systems using density-functional theory. *Comput. Phys. Commun.* **119,** 67–98 (1999).
32. Perdew, J. P., Burke, K. & Ernzerhof, M. Generalized gradient approximation made simple. *Phys. Rev. Lett.* **77,** 3865–3868 (1996).
33. Lindhard, J. & Scharff, M. Energy dissipation by ions in the kev region. *Phys. Rev.* **124,** 128–130 (1961).

Acknowledgements

Financial support from the DFG (SFB 616: Energy dissipation at surfaces; and SFB 445: Nanoparticles from the Gas Phase) by GANIL (Project S18), and the sixth framework programme of the EU (EURONS: RII3-CT-2004-506065) is gratefully acknowledged. We thank P. and F. Jeanjean for their help with the experiment and A. Reichert for discussions.
Correspondence and requests for materials should be addressed to M.S.

Author contributions

M.S. and H.L. conceived and designed the experiment. E.A., T.P., M.K., I.M., H.L. and M.S. performed the experiment and analysed and interpreted the data. E.A., R.M. and A.D. performed the theoretical calculations. All authors discussed the results and commented on the manuscript.

Competing financial interests

The authors declare no competing financial interests.